**Biomaterials
Science**

Enhanced transcellular penetration and drug delivery by crosslinked polymeric micelles into pancreatic multicellular tumor spheroids

**SCHOLARONE™
Manuscripts**

Graphic Abstract for

Enhanced transcellular penetration and drug delivery by crosslinked polymeric micelles into pancreatic multicellular tumor spheroids

Hongxu Lu, Robert H. Utama, Uraiphan Kitiyotsawat, Krzysztof Babiuch, Yanyan Jiang, Martina H. Stenzel

Transcellular penetration in multicellular tumor spheroids
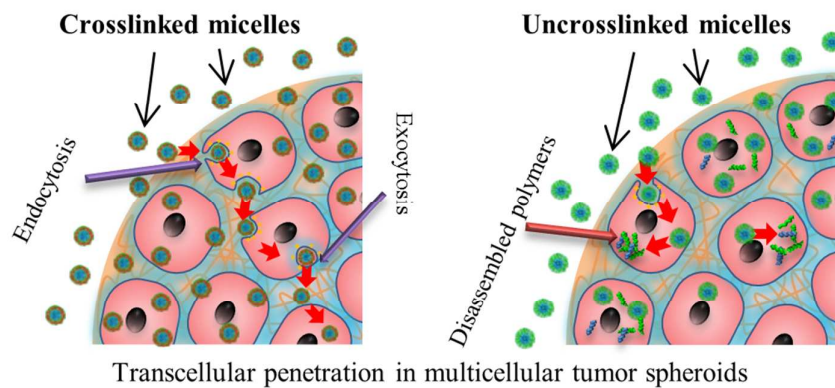
The penetration pathway of polymeric micelles into multicellular tumor spheroids (MCTS) depends on transcellular transport from peripheral cell into the inner cells. Stabilization by crosslinking of micelles facilitated the penetration into MCTS.

Biomaterials Science

ARTICLE

Enhanced transcellular penetration and drug delivery by crosslinked polymeric micelles into pancreatic multicellular tumor spheroids

Hongxu Lu,[a] Robert H. Utama,[a] Uraiphan Kitiyotsawat,[a,b] Krzysztof Babiuch,[a] Yanyan Jiang,[b] Martina H. Stenzel* [a]

Many attempts have been made in the application of multicellular tumor spheroids (MCTS) as a 3D tumor model to investigate their biological responses upon introduction of polymeric micelles as nanocarriers for therapeutic applications. However, the micelle penetration pathways in MCTS are not yet known. In this study, micelles (uncrosslinked, UCM) were prepared by self-assembly of block copolymer poly(N-(2-hydroxypropyl methacrylamide-*co*-methacrylic acid)-*block*-poly(methyl methacrylate) (P(HPMA-*co*-MAA)-*b*-PMMA). Subsequently, the shells were crosslinked to form relatively stable micelles (CKM). Both UCM and CKM penetrated deeper and delivered more Doxorubicin (DOX) into MCTS than the diffusion of the free DOX. Additionally, CKM revealed higher delivery efficiency than UCM. The inhibition of caveolae-mediated endocytosis, by Filipin treatment, decreased the uptake and penetration of the micelles into MCTS. Treatment with Exol, an exocytosis inhibitor, produced the same effect. Furthermore, movement of the micelles through the extracellular matrices (ECM), as modelled using collagen micro-spheroids, appeared to be limited to the peripheral layer of the collagen spheroids. Those results indicate that penetration of P(HPMA-*co*-MAA)-*b*-PMMA micelles depended more on transcellular transport than on diffusion through ECM between the cells. DOX-loaded CKM inhibited MCTS growth more than the UCM counterpart, due to possible cessation of endocytosis and exocytosis in the apoptotic peripheral cells, caused by faster release of DOX from UCM.

Introduction

Block copolymer micelles are water-soluble, biocompatible nanocarriers, which have frequently been used to carry, protect and deliver potential therapeutic molecules to solid tumors.[1-3] Micelles from amphiphilic block copolymers are typically spherical and nanosized (10 – 100 nm) self-assemblies that possess a core-shell type architecture.[4] Polymeric micelles enable the preferential delivery of drugs to tumors owing to the enhanced permeability and retention (EPR) effect.[5] It has been reported that they can overcome the inherent multidrug resistance of tumors against chemotherapeutics.[1] The hydrophilic outer shell prevents protein adsorption, thereby enhancing drug circulation time and the hydrophobic core serves as a nanocontainer of drugs protecting them from *in vivo* milieu. The drug-release kinetics can be controlled and the micelles can be modified with specific binding groups to target specific cancer cells or tumor microenvironments.[6] Both pre-clinical and clinical studies have demonstrated that micelles prepared from block copolymers incorporating doxorubicin (DOX), paclitaxel, or cisplatin drugs can reduce the toxic side effects of the loaded drug while maintaining appreciable antitumor efficacy.[7-11]

The majority of *in vitro* biological studies on micellar nanocarriers have been performed using two-dimensional (2D) monolayer cell cultures even though such suboptimal models might result in misleading observations and conclusions.[12] In order to reduce experimental uncertainties arising from monolayer cultures and from complicating factors such as pharmacokinetics and hepatic metabolism in animal studies, more attempts have been made to develop three-dimensional (3D) cell culture models to bridge the gap between 2D cell-based assays and *in vivo* studies.[13] One such model is the multicellular tumor spheroid (MCTS), fabricated by using the self-assembly process of cells in suspension.[14] Most MCTS exhibit higher similarity to real tissues in terms of 3D structure, cell metabolism and gene profiles than cell monolayers and

have therefore recently gained increasing recognition in biomedical research.[1, 12]

In attempts to make nanocarriers even more effective, researchers have prepared various nanoparticles, such as antibody-modified micelles,[15] receptor specific ligand-modified nanoparticles[16] as well as pH responsive liposomes.[17, 18] Recent studies have shown that modified micelles can penetrate deeper and deliver more drugs into MCTS resulting in higher toxicity to the spheroids.[15-21] However, one important factor that has been ignored is the micelle trafficking inside the MCTS, which revolves around how micelles pass through the peripheral cells and their surrounding extracellular matrix (ECM) networks. Due to the abnormal vascular structure of the tumor tissue, this population of cells has a typical distance of more than 100 μm from the blood vessel.[22] The ECM of solid tumors presents a transport barrier that restricts nanoparticle penetration and limits the efficacy of drug delivery. Detailed knowledge of the mode of penetration is invaluable as this information could be used to improve the efficiency of nano-sized drug carriers.

Micelles and other self-assembled aggregates are dynamic structures that can change size or disassemble into single amphiphilic molecules upon influences from the environment. Stabilization of micelles by crosslinking can prevent disassembly, which directly translates into an improved cellular uptake,[23] as well as prolonged circulation time *in-vivo*.[24] The aim of this study, in addition to the determination of the mode of micellar transport inside the MCTS, is to compare the penetration and drug delivery properties between self-assembled, uncrosslinked micelles (UCM) and shell-crosslinked micelles (CKM) inside the MCTS. The significance of the comparison of these two types of micelles is that they can be seen as representatives of a solid and stable system on one side and potentially degradable nanoparticles that may easily disintegrate on the other.

In this study, we selected a micelle model based on the block copolymer poly(*N*-(2-hydroxypropyl methacrylamide-*co*-methacrylic acid)-*block*-poly(methyl methacrylate) (P(HPMA-*co*-MAA)-*b*-PMMA) since PHPMA has been already tested in clinical trials as a drug carrier.[25] UCM were formed by self-assembly of P(HPMA-*co*-MAA)-*b*-PMMA. The hydrophilic shell of UCM was then crosslinked with a diamine (1,8-diaminooctane) to form CKM. The penetration and trafficking of CKM and UCM were first investigated with pancreatic MCTS, which were prepared from pancreatic cancer cell line AsPC-1. Different inhibitors were applied to study the internalization pathways of the micelles in the MCTS. Furthermore, DOX was encapsulated into the micelles to compare the differences of antitumor efficacy between CKM and UCM and to provide evidence for the proposed hypothesis of penetration mechanism on PHPMA-based micelles. In addition, MCTS prepared from human lung carcinoma A549 cells were also applied in this study in order to broad the applicability of the findings.

Materials and methods

Materials

All materials were reagent grade and used as received, unless otherwise specified: *N*-(2-Hydroxypropyl) methacrylamide (HPMA, Polysciences), fluorescein *O*-methacrylate (97%, Sigma-Aldrich), *N,N*-dimethylacetamide (DMAc, 99.9%, Sigma-Aldrich), diethyl ether (99%, Univar), methanol (HPLC grade, Ajax) and *N,N*-dimethylformamide (DMF, > 99.8%, Sigma Aldrich) were used without further purification. Methacrylic Acid (> 99%, Sigma-Aldrich) and methyl methacrylate (MMA, 99% Sigma-Aldrich) were de-inhibited by passing through a column of activated basic alumina. De-inhibited monomers were stored at below 4 ℃ and used within 7 d. 2,2'-Azobisisobutyronitrile (AIBN) was re-crystallized twice from methanol. Deionized (DI) water was produced by a Milli-Q reverse osmosis system and had a resistivity of 19.6 mΩ cm^{-1}. The RAFT agent, 4-cyano-4-methyl-4-thiobenzoylsulfonyl-butyric acid 2-(2,2-dimethoxy-ethoxy) ethyl ester (acetal-RAFT) was synthesized according to the literature.[26] Doxorubicin HCl solution (Andriamycin®, Pfizer Australia) was provided by Dr. Hien Duong and Dr. Cyrille Boyer in the Centre for Advanced Macromolecular Design at the University of New South Wales. Collagen solution (type I), Nile Red (≥ 98%), Chlorpromazine hydrochloride (≥ 98%), Filipin (Filipin III, ≥ 85%), Amiloride (≥ 98%), NaN$_3$ and 2-Deoxy-D-glucose (≥ 98%) were all obtained from Sigma-Aldrich. Exo1 (2-[(4-Fluorobenzoyl)amino]benzoic acid methyl ester) was purchased from Enzo Life Sciences (Farmingdale, NY).

Synthesis of [P(HPMA-*co*-MAA)-*b*-PMMA]

P(HPMA-*co*-MAA)-*b*-PMMA were synthesized using RAFT (Reversible Addition Fragmentation Chain Transfer) polymerization as shown in the Scheme 1. HPMA (1 g, 6.98 x 10^{-3} mol), MAA (0.200 g, 2.33 x 10^{-3} mol), acetal-RAFT (0.0319 g, 7.76 x 10^{-5} mol) and AIBN (2.55 mg, 1.52 x 10^{-5} mol) were dissolved in DMAc (5.68 mL) to give a [HPMA]:[MAA]:[RAFT]:[Initiator] ratio of 90:30:1:0.2. Fluorescein *O*-methacrylate (10 mg) was also added as the fluorescent label. The solution was thoroughly purged with nitrogen gas for 30 min before being placed in an oil bath at 70 ℃ and stirred for 7 h. After polymerization, the reaction was stopped by placing the solution in an ice bath for 30 min. The polymer was isolated by precipitation in diethyl ether to yield P(HPMA-*co*-MAA). The conversion for HPMA and MAA was determined to be 27% and 38% respectively *via* ^{1}H NMR (D$_2$O) (Supplementary Fig. 1). P(HPMA-*co*-MAA) (0.346 g, 7.52 x 10^{-5} mol) was employed as a macroRAFT agent, mixed with MMA (0.753 g, 7.52 x 10^{-3} mol) and AIBN (2.47 mg, 1.50 x 10^{-5} mol) in DMAc (7.89 ml) to give a [monomer]:[macroRAFT]:[initiator] ratio of 100:1:0.2. The solution was thoroughly degassed in an ice bath for 30 min before being placed in an oil bath at 70 ℃ and stirred for 6 h. The polymerization was stopped by placing the solution in an ice bath for 30 min. The final solution was then precipitated in methanol to yield a brittle, pink solid. The monomer conversion was 39 % by ^{1}H NMR (CDCl$_3$) (Supplementary Fig. 2). ^{1}H NMR spectroscopy was carried out using a Bruker Avance III 300 MHz, equipped with an auto sampler system. Chemical shifts are reported in parts per million (ppm), relative to the residual solvent peak. The theoretical molecular weight ($M_{n, th}$) was calculated according to the following equation: $M_{n,th} =$

$\frac{[Monomer]}{[RAFT]} \times Conversion \times M_{monomer} + M_{RAFT}$. M_{RAFT} stands for the molecular weight of the RAFT agent or the macroRAFT agent.
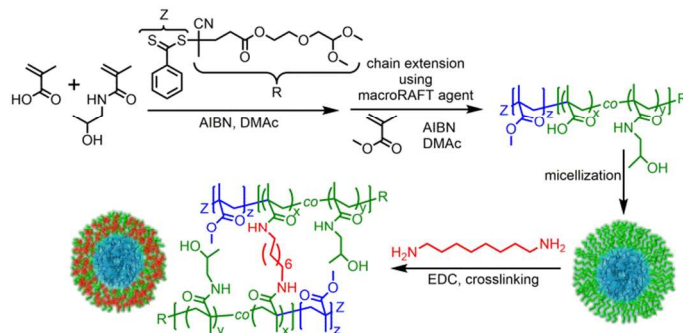
Scheme 1 Schematic representation of the synthesis of block copolymer and formation of UCM and CKM.

Preparation of micelles from block copolymer and shell-crosslinking

10 mg of P(HPMA-*co*-MAA)-*b*-PMMA was dissolved in 2.5 mL of DMF. Deionized (DI) water (5 mL) was added drop wise to the DMF solution using a syringe pump (0.7 mL/h). The samples were dialyzed against DI water for 9 h using membrane with a cutoff of 6000 - 8000. Water was replaced every hour. 1 mg of 1,8-diaminooctane (Sigma Aldrich) and 1 mg of l-ethyl-3-(3'-dimethylaminopropyl)-carbodiimide hydrochloride (EDC) (Sigma Aldrich) were added to UCM and incubated overnight to generate CKM according to the previously described method.[27]. The residue of 1,8-diaminooctane and EDC was removed by dialysis. The micelles were analyzed using Dynamic Light Scattering (DLS) and Transmission Electron Microscopy (TEM). DLS analyses were run on a Zetasizer Nano ZS (Malvern), with a 4 mV He-Ne laser operating at $\lambda = 632$ nm and non-invasive backscatter detection at 173 °. Measurements were conducted in a Quartz cuvette with 30 s equilibration period prior to each set of measurements. Samples were passed through 0.45 μm filters before analyzing, and measured three times at 25 °C. The TEM micrographs were obtained using a FEI Tecnai G2 20 TEM transmission electron microscope. The instrument operates at an accelerating voltage of 200 kV. Samples were negatively stained with uranyl acetate (2 w/w %). The particles were cast onto a Formvar-coated grid by placing a droplet of the aqueous micelle solution for 15 min onto its surface, followed by the removal of excess solution using filter paper. In the staining process, the cast grid was gently laid onto the surface of a drop of uranyl acetate for 1 min. The stained grids were dried under air.

Drug loading into micelles

The dialysis method was used to load model drug Nile Red into the micelles. Initially, polymers and Nile Red were dissolved in 2.5 mL DMF and incubated for 1 h, followed by drop wise addition of 5 mL DI water using a syringe pump. The solution was dialyzed against DI water (MWCO 6000-8000) for 9 h.

The anti-cancer drug DOX was also loaded to CKM and UCM. Firstly, Doxorubicin HCl solution (Andriamycin®, Pfizer Australia) was lyophilized for 24 h. The DOX powder was dissolved in DMF at a concentration of 1 mg/mL.

Triethylamine was added for neutralization (1 μL per mL DMF) and to improve the loading efficiency of DOX into the micelles.[28] Polymer was dissolved in DMF and mixed with DOX for 1 h. DI water was added dropwise into the polymer-DOX mixture to encapsulate the drug in the micelles. The solution was dialyzed (MWCO 6000-8000) against DI water for 9 h. The loading of DOX into the polymeric micelles was determined by reading the absorbance intensity at 480 nm using a Cary 300 Scan UV-vis spectrophotometer (Agilent Technologies) based on a DOX standard curve. Drug loading efficiency (DLE) was calculated according to the following equation:$DLE =$
$(DOX\ in\ micelles)/(DOX\ added\ initially) \times 100\%$.

The release of DOX from the micelles was studied by dialysing the micelles against a citrate buffer solution (10 mM, pH 5.0) or a phosphate buffer solution (10 mM, pH 7.4). At regular time points, samples in the dialysis tube were taken and the concentrations of DOX in the micelles were determined by UV-vis spectrophotometry. The percentages of released drug were calculated as the ratio of released DOX to DOX at t_0.

Collagen micro-spheroid formation and collagen-coated TCPS

Collagen micro-spheroids were prepared using the method described by Matsunaga *et al*[29] with some modifications. Type I collagen (Sigma-Aldrich) was neutralized with NaOH at 4 ºC and diluted to 2 mg/mL in PBS. The neutralized collagen solution was added drop wise into rice oil with lecithin (2%) by hand. The droplets were incubated at 37 °C for 1 h for gelation of the collagen with constant rotating. Hexadecane plus Span 80 (2%) was added to dissolve the remaining oil. After aspirating the hexadecane, the collagen micro-spheroids were washed three times with a buffer solution (RPMI 1640 medium with 0.1% Tween 20). The collagen spheroids were pipetted into a 35 mm glass bottom dish and incubated with micelles (100 μg/mL) for 1 h before confocal microscopic observation.

To coat the TCPS, the neutralized collagen solution (0.2 mg/mL) was pipetted to 24 well plates (200 μL per well). After air drying for 24 h, 0.5 mL micelles (100 μg/mL) was added to the wells and incubated for 1 h before washing thrice with PBS. The micelle and washing solution was collected and the fluorescence intensity was recorded using the spectrofluorometer.

AsPC-1 MCTS preparation and characterisation

AsPC-1 cells were obtained from European Collection of Cell Cultures (ECACC) via Australian Cell Bank. AsPC-1 cells were cultured in T-25 cell culture flask with 5 % CO$_2$ at 37 ºC. The cells were cultured in RPMI1640 supplemented with 10% fetal bovine serum, 100 U/mL penicillin, 100 μg/mL streptomycin, and 1 mM sodium pyruvate. After the cells reached confluence, the cells were washed with phosphate buffered saline (PBS) and detached by trypsin/EDTA treatment. The cells were collected, centrifuged and resuspended in the culture medium.

The cell density of the cell suspension was adjusted to 1.0×10^5 cells/mL. 10 μL of cell suspension was gently dropped on to the lid of a 100 mm cell culture dish. The lid was then slowly turned over and placed onto the dish, which was filled with 10 mL sterile PBS to maintain the humidity of inner dish chamber. The cells were incubated and kept undisturbed at 37 ºC with 5

% CO_2 to form spheroids. After culture for 7 days, the MCTS were transferred to a 96-well suspension culture plate (Corning) and cultured for 1 day before further experiments. The morphology of the MCTS was recorded using a Leica DM IL inverted microscope equipped with a ProgRes® Scan camera (Warner Instruments, LLC) and the sizes were analyzed using the software ProgRes® CapturePro.

The cell number of the MCTS was investigated by measuring the DNA contents. Spheroids were collected in a 1.5 mL centrifuge tube, washed thrice with PBS and rinsed with MilliQ water. The spheroids were lyophilized and dispersed in 200 µL lysis buffer (0.5% sodium dodecyl sulfate (SDS) in 50 mM Tris, pH 8.0) overnight at 4 °C. An aliquot of lysate was used to measure the DNA content of MCTS with Hoechst 33258 based DNA Quantitation Kit (Sigma-Aldrich) under a Cary Eclipse Fluorescence Spectrophotometer (Agilent Technologies) at excitation = 360 nm and emission = 460 nm. The fluorescence values were used to calculate cell numbers based on a standard curve made from the lysate of serial numbers of AsPC-1 cells.

Micellar penetration observed with laser scanning confocal microscopy (LSCM)

For confocal microscopy observation, the spheroids were first treated with micelles (75 µg/mL) for 1 h. After incubation, the spheroids were washed thrice with PBS. Finally, the cells were mounted in PBS and observed under a laser scanning confocal microscope (Zeiss LSM 780). The system is equipped with a Diode 405-30 laser, an argon laser and a DPSS 561-10 laser connected to a Zeiss Axio Observer.Z1 inverted microscope. The ZEN2011 imaging software (Zeiss) was used for image acquisition and processing. In Figure 4B, the spheroids were stained with 2.0 µg/mL Hoechst 33342 (Invitrogen) for 5 min and washed thrice with PBS before observation.

Endocytosis and exocytosis inhibitor treatment

The spheroids were pre-incubated for 30 min at 37 °C with various endocytosis inhibitors: Chlorpromazine (10 µg/mL), Filipin (10 µg/mL), Amiloride (50 µM) and NaN_3 + deoxyglucose (5 mM + 5 mM) solution.[11, 30, 31] Those inhibitors showed no acute toxicity to the cells in the *in vitro* cytotoxicity tests (Supplementary Methods and Supplementary Fig. 3). The micellar solutions (final concentration of 75 µg/mL) were added to the spheroids and incubated for 2 h at 37 °C in 5% CO_2. The same concentrations of inhibitors were present during the incubation with the micelles. The spheroids were washed 2 times with PBS. The uptake of micelles by the MCTS was quantified by measuring the fluorescence intensity of the micelle solution together with the washing PBS using a Cary Eclipse Fluorescence Spectrophotometer (Agilent Technologies) at λex = 490 nm and λem = 512 nm. The values were then compared to the fluorescence intensity of the solution at time 0. The experiments were carried out in quadruplicate.

The spheroids were also pre-incubated for 30 min at 37 °C with exocytosis inhibitor Exo1 (100 µM). Exo1 showed no acute toxicity to AsPC-1 cells (Supplementary Fig. 3). The micellar solutions (final concentration of 75 µg/mL + 100 µM Exo1) were added to the spheroids and incubated for 2 h at 37 °C in 5% CO_2. The spheroids were then washed 3 times with PBS and mounted in PBS for LSCM observation. The influences of Exo1 on the micellar uptake by AsPC-1 cells were tested using 2D cultured cells. AsPC-1 cells were seeded in 24 well plates at

1×10^5 cells per well and incubated for 2 days before treatment. The cells were firstly pre-treated with 100 µM Exo1 in cell culture medium for 30 min before incubation with 100 µg/mL micelles (supplemented with 100 µM Exo1) for 1 h. The cells were then washed with PBS twice. The fluorescence intensity of medium together with washing PBS, which indicates the remaining micelles, was measured using the fluorescence spectrophotometer.

Treatment of MCTS with DOX-loaded micelles

Doxorubicin distribution and accumulation
DOX-loaded CKM, UCM and free DOX were added to the pancreatic MCTS, which have been cultured for 1 day in 96-well suspension culture plates. The distribution of DOX in MCTS after treatment for 2 h was observed with LSCM. In addition, DOX distribution was investigated with MCTS of A549 cells. The preparation of method for A549 MCTS was as same as that for AsPC-1 cells except the cell density of the cell suspension was adjusted to 1.5×10^5 cells/mL. After culture for 7 days, the A549 MCTS were transferred to a 96-well suspension culture plate and cultured for 1 day.

Doxorubicin accumulation in AsPC-1 spheroids was evaluated by fluorescence according to the reported methods.[15, 32] Spheroids were incubated with free doxorubicin or DOX-loaded micelles for 12 h. Six spheroids from each sample group were collected into a 1.5 mL centrifuge tube, washed with PBS thrice and rinsed with MilliQ water. The spheroids were lyophilized and dispersed in 200 µL lysis buffer (0.5% sodium dodecyl sulfate (SDS) in 50 mM Tris, pH 8.0) overnight at 4 °C. The amount of doxorubicin was estimated by absorbance with the UV-Vis spectrophotometer (Cary 300 Scan) at 480 nm based on doxorubicin standards in dialysis buffer. Micellar doxorubicin formulations were used at equivalent concentrations of free doxorubicin.

Inhibition of MCTS proliferation
The pancreatic MCTS after DOX and micellar treatment for 7 d were harvested to measure the DNA contents. The spheroids were first treated with lysis buffer using the above method. An aliquot of lysate was used to measure the DNA content of MCTS with Hoechst 33258 based DNA Quantitation Kit (Sigma-Aldrich) under a Cary Eclipse Fluorescence Spectrophotometer (Agilent Technologies) at excitation = 360 nm and emission = 460 nm. The fluorescence values were used to calculate DNA contents based on a standard curve made from the standard DNA provided with the kit.

Statistical analysis

All data were reported as mean ± standard deviation (SD). A student *t*-test was used in Figure 3C, 4C, 5A to reveal the statistical differences. For all the other data, a one-way analysis of variance was performed for the statistical analysis followed by a Tukey's post hoc test for pairwise comparison. A p value less than 0.05 was considered statistically significant. All the statistical analysis was done with GraphPad Prism 6.0.

Results and discussion

Polymer synthesis, micelle formation and Nile Red loading

P(HPMA-*co*-MAA)-*b*-PMMA was synthesized using RAFT polymerization as shown in the scheme in Scheme 1. UCM were prepared by dissolving the copolymers in DMF, followed by drop wise addition of distilled water, which resulted in the formation of micelles with hydrophobic PMMA in the core and hydrophilic P(HPMA-*co*-MAA) in the shell. UCM were subsequently shell-crosslinked using 1,8-diaminooctane and EDC to form CKM. Both micelles exhibited spherical morphologies under TEM (Fig. 1A). The TEM images revealed the diameters of the micelles to be in the range of 30 nm. The DLS measurements further confirmed the similar hydrodynamic diameters of approximately 30 nm for both UCM and CKM, with a narrow distribution (Fig. 1B). The zeta-potential of UCM was −7.8 mV in water, which is more negative than that of CKM (−1.5 mV). The micelle cytotoxicity was evaluated with AsPC-1 cells revealing no toxicity observed, within the range of tested concentrations (2 − 250 g/mL) with either CKM or UCM (Supplementary Fig. 4). A fluorescent dye, Nile Red, was loaded into the micelles. The hydrodynamic diameters of Nile Red-loaded UCM (UCM-n) and CKM (CKM-n) were 36.45 ± 0.51 and 36.34 ± 0.22 nm, respectively.
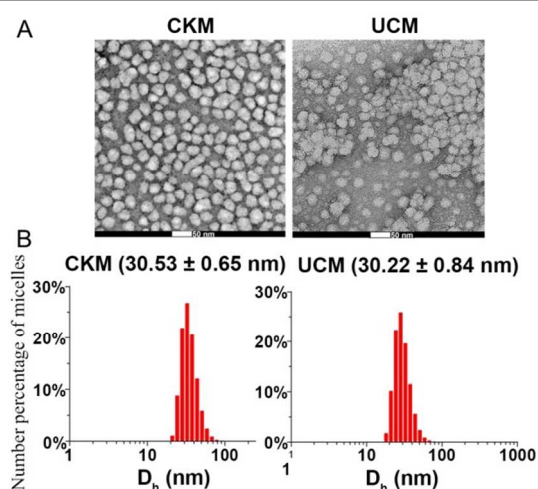
Fig. 1 TEM micrographs of CKM and UCM (A) and hydrodynamic diameter (D_H) distributions of CKM and UCM revealed by DLS (B). Scale bar = 50 nm.

Enhanced penetration and delivery by polymeric micelles into pancreatic MCTS

The pancreatic MCTS were prepared with human pancreatic carcinoma AsPC-1 cells using a hanging drop method. The AsPC-1 spheroid has a diameter of approximately 350 μm after hanging in the medium drop for 7 d. There were about 3,800 cells in one AsPC-1 spheroid, packing in a sphere of 0.03 mm^3 according to the DNA quantification results. The MCTS were cultured for 1 d in 96-well suspension culture plates before exposed to micelles or free drugs. The MCTS were incubated with Nile Red-loaded micelles (CKM-n and UCM-n) for 2 h. The micelle penetration and distribution of Nile Red, as a model drug, were observed with LSCM. The LSCM optical cross-sections of MCTS at the depth of 90 μm are shown in

Fig. 2. CKM penetrated deeper into the MCTS than UCM. The deeper penetration of CKM subsequently resulted in a higher penetration of the model drug. Compared with free Nile Red, both CKM and UCM delivered more Nile Red further into the spheroid.
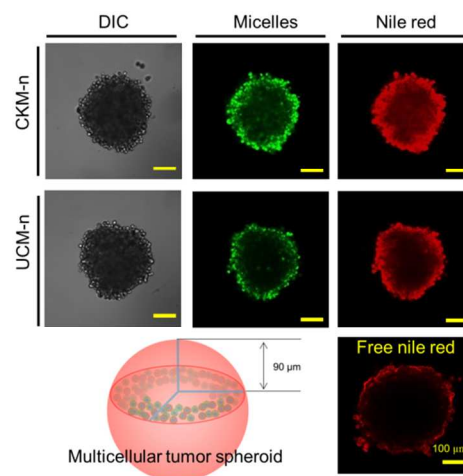
Fig. 2 Laser scanning confocal microphotographs revealed the deeper model drug delivery into MCTS induced by the deeper penetration of micelles. Scale bar = 100 μm. DIC, Differential interference contrast images. CKM-n and UCM-n, Nile Red-encapsulated CKM and UCM, respectively. The polymer was labeled with fluorescein to enable fluorescent visualization.

Limited micelle diffusion in collagen micro-spheroids

One possible pathway of the deeper penetration of P(HPMA-*co*-MAA)-*b*-PMMA micelles (compared with free Nile Red) is that micelles diffuse into pancreatic MCTS through the collagen-rich ECM molecular network. To confirm this pathway, the micelle diffusion ability in the ECM was investigated with collagen micro-spheroids fabricated with the reported method[29] with some modifications. The collagen spheroids had a diameter of about 400 μm in PBS. As shown in Fig. 3A, both CKM and UCM had the same diffusion distance (20 ~ 30 μm) into the peripheral layer of the collagen micro spheroids. The results were similar to the diffusion of free Nile Red, however, more superficial than the penetration of the polymeric micelles in pancreatic MCTS.

Furthermore, we evaluated the collagen adsorption of UCM and CKM using a 2D collagen-coated tissue culture plate surface (Col-TCPS) model (Fig. 3B). After the exposure of Col-TCPS to micelle suspensions for 1 h, the fluorescence intensities (FI) of the supernatant were measured. The obtained values correlated with the concentration of the micelles which were not absorbed by the Col-TCPS. There was no clear difference between FI observed before and after exposed and no statistical difference was observed between Col-coated TCPS and TCPS.

Those results indicated that the ECM acts more as a barrier for micelle penetration and does not facilitate the diffusion, and hence the penetration of micelles in MCTS. Thus, the deeper penetration of micelles might be enabled by the cells and their

activity in MCTS. The reason for the penetration difference between CKM and UCM could then be attributed to the changes in endocytosis and exocytosis (transcytosis) of the nanoparticles.
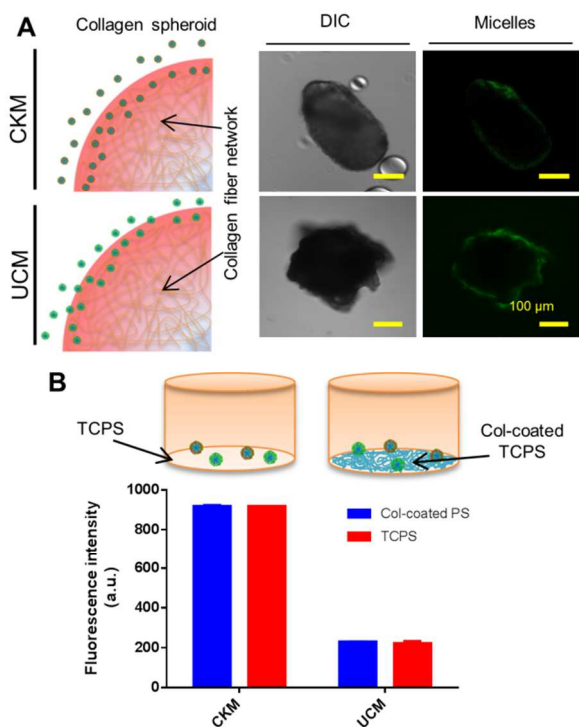
Fig. 3. Micelle penetration in collagen micro spheroids (A) and micelle adhesion on col-coated TCPS (B). (A) Distribution of CKM and UCM in the collagen spheroids observed with LSCM. Scale bar = 100 µm. (B) The adsorption of CKM and UCM by TCPS and collagen-coated TCPS. Data represent mean ± SD, n = 3.

Micelle penetration in MCTS via transcellular transport

Since the penetration enhancement of micelles was not facilitated by diffusion through ECM, our hypothesis of the deeper penetration of micelles is due to the transcellular transport of micelles by cells from the outer layer to the inner part of MCTS (Fig. 4A). In this transcellular transport, the cells in the peripheral layer of MCTS uptake micelles from the surrounding milieu and then partially release the micelles into the inner parts of MCTS via exocytosis. In the ECM of the inner part of MCTS, the micelles exocytosed by cells were observed using LSCM and are shown in Fig. 4B. Our previous results[27] have demonstrated that the cells can release micelles via exocytosis, and that exocytosis is significantly enhanced when the micelles are shell-crosslinked.

To confirm the hypothesis, we first blocked micelle uptake by applying various endocytosis inhibitors. The internalization pathways include clathrin-mediated endocytosis, caveolae-mediated endocytosis, clathrin- and caveolae-independent endocytosis, phagocytosis, and macropinocytosis.[33] The mechanisms of nanoparticle internalization have been extensively investigated with 2D monolayer cell culture

models[4] but, to the best of our knowledge; have never been investigated in a MCTS model. Here, chlorpromazine (CPZ), Filipin, Amiloride (AMR) and sodium azide plus deoxyglucose (NaN_3+DG) were used to inhibit the clathrin-mediated, caveolae-mediated, macropinocytosis, and energy-dependent endocytosis pathways, respectively. MCTS were pre-treated with various inhibitors for 30 min in serum free cell culture medium before incubation with micelle suspensions (75 µg/mL) for 2 h. Fluorescence intensities of the supernatants, which indicate the amounts of non-internalized micelles, were measured to calculate the uptake ratios, as described in the experimental section. As shown in Fig. 4C, about 12% of CKM and 15% of UCM were taken up by the pancreatic MCTS. When treated with Filipin and NaN_3+DG, the internalization ratios of both CKM and UCM were significantly decreased, as compared to the other inhibitor groups. These results showed that Filipin and NaN_3+DG hampered the uptake of both CKM and UCM. Although the inhibitory effect of NaN_3+DG was higher than that of Filipin, there was no statistical difference between these two inhibitors. The molecular size of NaN_3, a small inorganic salt, is much lower than Filipin, a large macrolide ring structure, which may cause NaN_3 to diffuse deeper and faster than Filipin. Therefore, the inhibition effect of the salt was higher than of the macrolide. The inhibitory effects were also confirmed with LSCM. In Fig. 4D, both the FI and penetration depth of CKM and UCM had clearly decreased after Filipin or NaN_3+DG treatments, as compared with the untreated control (Fig. 2A). Additionally, in order to exclude the uptake decrease due to cytotoxicity, the cell viability after treated with the applied concentrations of inhibitors was tested with a WST-1 assay. None of the examined compounds revealed any acute toxicity toward AsPC-1 2D cell cultures (Supplementary Fig. 3).
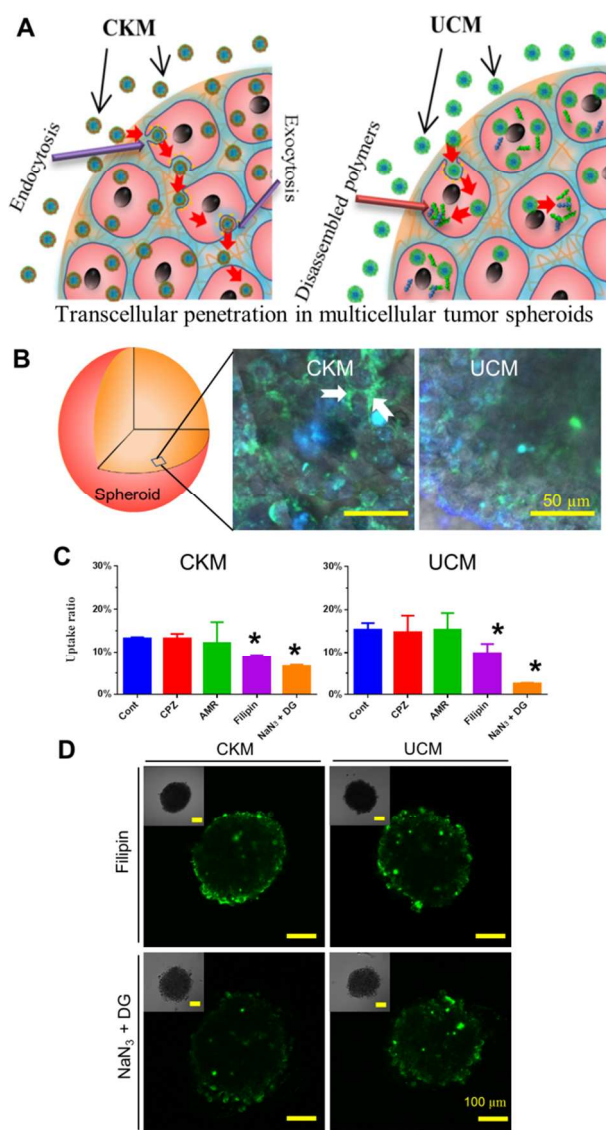
Fig. 4. Penetration pathway of CKM and UCM into pancreatic spheroids. (A) Schematic images of different penetration pathways for CKM and UCM. (B) Higher magnification of confocal images showed the distribution of CKM (arrows) in the spaces (ECM) among cells in the MCTS. Scale bar = 50 µm. (C) Micelle uptake in MCTS was decreased by different inhibitors. Data represent mean ± SD, n = 3. *, significant difference, $p < 0.05$. (D) Micelle uptake was inhibited by Filipin and NaN$_3$ + DG, as observed with LSCM. Scale bars = 100 µm.

We further treated MCTS with an exocytosis inhibitor Exo1. Exo1 has been reported to inhibit cell exocytosis by inducing rapid collapse of the Golgi apparatus to the endoplasmic reticulum.[34, 35] Exo1 showed no influence on the uptake amount of both CKM and UCM for AsPC-1 in monolayer culture (Fig. 5A). An *in vitro* cytotoxicity test also revealed that it has no influence on cell viability when AsPC-1 cells were exposed to 100 µM Exo1 for 90 min (Supplementary Fig. 3). As shown in Fig. 5B, the penetration of micelles obviously decreased when MCTS were treated with Exo1. The result that decrease of micellar penetration by endo- and exocytosis inhibitors indicates that the penetration mechanism

of our P(HPMA-*co*-MAA)-*b*-PMMA micelles heavily relies on the transcellular transport by endocytosis and exocytosis.
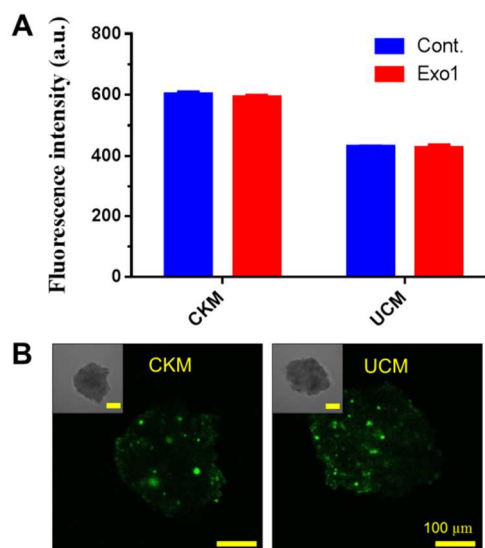
Fig. 5. Exo1 did not inhibit the uptake of both CKM and UCK in the 2D cultured AsPC-1 (A) and LSCM images of the micellar penetration into pancreatic MCTS after treatment with Exo1. (A) The fluorescence intensity indicates the micelles in the supernatant. (B) The insets show the differential interference contrast images of the MCTS. Scale bars = 100 µm.

Apoptotic peripheral cell layer hindered micelle penetration in MCTS

A further experiment with anti-cancer drug DOX-loaded into micelles was carried out to examine our hypothesis. DOX has been widely used as a promising agent for cancer therapy. DOX can cause apoptosis of cancer cells and various nanoparticles including micelles have been used as carriers for DOX.[28, 32] Based on our hypothesis, it is stipulated that faster release of DOX from un-crosslinked micelles will cause faster apoptosis of outer cells and cease the trancytosis of micelles into pancreatic MCTS (Fig. 6). It will lead to a compromised inhibition effects on the MCTS proliferation for the DOX-loaded UCM.
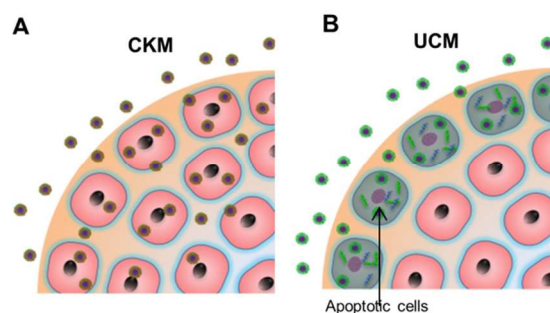
Fig. 6 Schematic hypothesis of penetration differences for DOX-loaded CKM and UCM.

Two concentrations of DOX were encapsulated into micelles by drop wise addition of water into the organic solution of polymer

and DOX followed by dialysis against distilled water and crosslinking for CKM. When the drug/polymer mass ratio was 5:1, the drug loading efficiency (DLE) was 30.4% and 34.1% in CKM-h and UCM-h, respectively. The drug/polymer mass ratio of 25:1 resulted in DLE of 42.2% (CKM-l) and 43.9% (UCM-l) (Table 1). The diameters of DOX-loaded UCM and CKM were 39.49 ± 0.80 and 35.78 ± 0.20 nm, respectively. The DOX release profiles of both CKM and UCM are shown in Supplementary Fig. 5. UCM showed a faster release than CKM at both pH 7.4 and pH 5.0. UCM released 83.3% of DOX at pH 5.0 after incubation for 2 h; while 53.3% of DOX was released at pH 7.4. Low pH also accelerated DOX release from CKM. At pH 5.0, CKM released 69.8% of DOX after 48 h (25.8% at pH7.4).

Table 1 DOX loading efficiency of crosslinked and uncrosslinked micelles.

	Polymer : drug ratio	Drug loading efficiency (w/w %)	Drug mass fraction of polymer (w/w %)
CKM-h	1:5	30.4%	6.1%
UCM-h	1:5	34.1%	6.8%
CKM-l	1:25	42.2%	1.7%
UCM-l	1:25	43.9%	1.8%

DOX-loaded micelles or free DOX were administrated to the pancreatic MCTS. The DOX concentrations were adjusted to 20 µM for CKM-h and UCM-h and to 5 µM for CKM-l and UCM-l. Free DOX was also administrated to the MCTS at 20 µM (DOX-h) and 5 µM (DOX-l). After being incubated with free DOX or DOX-micelles for 2 h, the MCTS were washed with PBS and the distribution of DOX inside MCTS was observed using LSCM (Fig. 7A). It was found that although both of them had a deeper penetration than free DOX, the crosslinked micelles carried DOX deeper than uncrosslinked ones. It was reported that MCTS exhibit disparate properties when compositional cells are different.[36] In order to boarder our hypothesis about micelle penetration in MCTS, we prepared another kind of MCTS from lung carcinoma A549 cells. A549 MCTS also showed a spherical morphology with a diameter about 300 µm. CKM and UCM showed a deeper delivery of DOX to A549 spheroids after incubation with CKM and UCM for 2 h (Supplementary Figure S7). And CKM delivered more DOX than did UCM. This indicates that the transcellular penetration of PHPMA based micelles may not only happen in pancreatic tumors but in other types of solid tumors.

The DOX uptake in the pancreatic MCTS after 6 h was quantified by absorbance measurements and the results are depicted in Fig. 7B. Both micellar systems showed improved penetration over free DOX alone. CKM-h delivered more DOX than all the other groups including UCM-h even though UCM-h had a higher DLE than CKM-h. A similar result was observed with CKM-l and UCM-l.
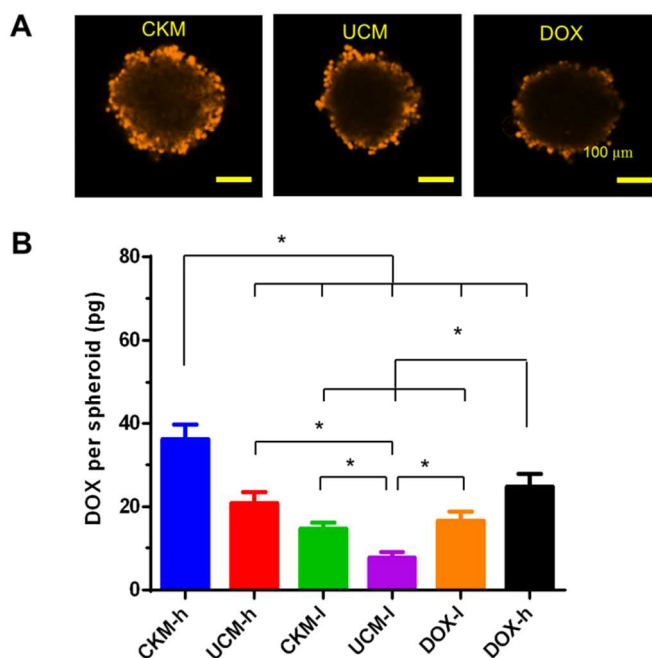
Fig. 7 DOX delivery into MCTS by CKM and UCM into pancreatic MCTS. (A) DOX delivery into MCTS by micelles revealed by LSCM. Scale bars = 100 µm. (B) Uptake amount of DOX by pancreatic MCTS after 12 h. Data represent mean ± SD, n = 3. *, significant difference, $p < 0.05$.

The MCTS were further incubated with free DOX or DOX-micelles for 7 d at 37 °C. The morphology of MCTS is shown in Fig. 8A and Supplementary Fig. 6. The MCTS were approximately of 350 µm before treatment (Fig. 8A, upper pattern). After expos to free DOX or DOX-micelles for 7 d, CKM-h showed an obvious inhibitory effect on the growth of MCTS (Fig. 8A, lower pattern). However, the sizes of MCTS in the other treatment groups increased by varying degrees. The sizes of the MCTS were quantitatively measured based on optical microphotographs and plotted in Fig. 8B. In the control group, the observed MCTS size increase was approximately 1.5-fold (from 350 µm to 550 µm) after 7 days of incubation. All the micellar treatment groups showed a lower size increase than free DOX. CKM showed a better inhibition effect than UCM. However, there is no obvious difference between DOX-h and DOX-l in the size changes. Furthermore, the DNA contents, which indicate cell numbers of MCTS, were measured with a Hoechst 33258 based DNA Quantitation Kit (Fig. 8C). After 7 days, CKM-h restrained cell proliferation and resulted in the lowest DNA content from all 7 groups. In addition, it was the only treatment that resulted in a decline in the cell number. The cells number increased in the sequence of CKM-h < UCM-h < CKM-l < UCM-l < DOX-h < DOX-h and control. The DNA contents of the MCTS subjected to the DOX-loaded, crosslinked micelles (CKM-h and CKM-l) were less than those of un-crosslinked micelles (UCM-h and UCM-l), as compared at the same DOX concentrations. Free DOX-h and DOX-l had similar spheroid size and DNA contents, which might be caused by the poor penetration of free DOX.
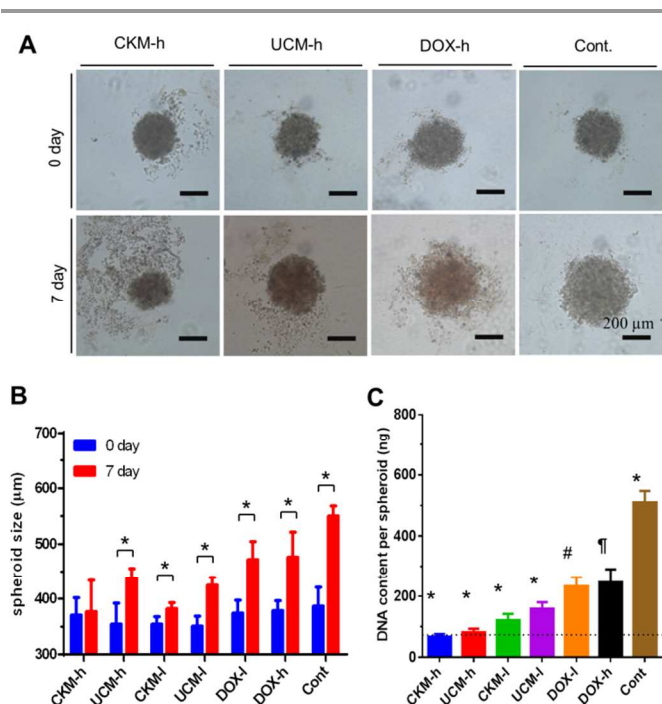
Fig. 8 Inhibition of the pancreatic MCTS growth by DOX-loaded micelles. (A) Microphotographs of pancreatic spheroids before and after DOX-loaded micelle treatments. Bar = 200 μm. (B) Size changes of MCTS during the drug or micelle treatments. Data represent mean ± SD, n=3. *, significant difference, $p < 0.05$. (C) DNA contents of pancreatic spheroids after DOX-loaded micelle treatment. The dashed line indicates DNA content before treatment (72.23 ng). Data represent mean ± SD, n=3. *, significant difference vs all the other groups, $p < 0.05$. #, significant difference vs all the other groups except DOX-h, $p < 0.05$. ¶, significant difference vs all the other groups except DOX-l, $p < 0.05$.

Polymeric micelles provide a promising tool for cancer therapies via precise and effective tumor-targeted drug delivery. Crosslinking has been considered as a useful approach to increase the stability[37] and blood circulation time of micelles.[24] This results in various micelles with significantly improved antitumor activity. Our previous results have demonstrated that shell-crosslinking can improve exocytosis of micelles because the un-crosslinked micelles will easily disassemble after internalization.[27] In a 2D cell monolayer model, micelles should be designed to disassemble and release the drug before exocytosis happens in order to reach the highest effect. In this study, our results revealed that in 3D MCTS, stabilization such as crosslinking plays a key role for the penetration of PHPMA-based micelles. The increased exocytosis into the spheroid improved the crosslinked micelle (CKM), and hence DOX, penetration. The fast release of antitumor drugs from UCM caused apoptosis of peripheral cells and stopped transcytosis of the micelles from the outer to the inner perimeter of the MCTS. These results highlight the importance of crosslinking for the design of PHPMA-based micelles for drug delivery. Furthermore, by the variation of crosslinking degree, optimization of the tumor penetration depth may be achieved. Ideally, through improvement of micelle stability, the encapsulated drug can be targeted into the inner core of the MCTS, whereby the particle will disassemble and release the therapeutic, thus, causing the apoptosis of cancer cells/tissues from inside out.

The size of the nanocarrier is of critical importance for tissue penetration and drug delivery.[20] Increasing the size of the nanoparticle will provide selectivity, but at the cost of limiting extravasation from some pores of tumor vessels and decreasing diffusion through the tumor matrix.[5] Nanoparticle-mediated cellular response is also size-dependent.[38] Nanoparticles less than 100 nm are usually considered as ideal drug carriers. Cabral *et al* demonstrated that only 30 nm poly(ethylene glycol)-*b*-poly(glutamic acid) micelles can accumulate in pancreatic tumors to achieve an antitumor effect.[8] Since both CKM and UCM have a very similar size (approximately 30 nm), it means that the micelle size had no influences on the cellular responses toward those two micelles.

Penetration of molecules and micelles in tumors depends on the volume fraction of the ECM components, particularly the collagen and glycosaminoglycan content. It has been reported by Albanese *et al.* that the 110 nm particles cannot penetrate into MCTS of MDS-MB-435 melanoma cells while 40 nm particles showed good penetration.[39] This observation could be related to the peripheral matrix that blocks the penetration of nanocarriers. Degradation of the collagen matrix with bacterial collagenase treatment in high collagen- content tumors caused significant increase of the interstitial distribution of nanoparticles. It has been reported that there was a 4-fold increase in the number of penetrating nanoparticles when the surface was immobilized with collagenase.[40] Therefore, the modification of CKM using ECM enzymes will be a useful method to increase penetration in MCTS. However, it should be mentioned that the ECM enzyme must be very carefully selected because degradation of some ECM molecules may slow down the penetration. Degraded ECM hyaluronan can increase the viscous hindrance and result in an inhibited diffusion of nanoparticles.[41]

Further studies are highly desirable to extend the application of the findings presented in this publication. In this report, even CKM-h failed to completely destroy the pancreatic MCTS. This was also seen in C6 glioma MCTS treated with PAMAM dendrimer-based DOX nanoparticles[42] and neuroblastoma MCTS treated with DOX-loaded iRGD-conjugated boronic acid-rich chitosan-poly(*N*-3-acrylamidophenylboronic acid) nanoparticles.[43] Although the growth of those MCTS was inhibited, the structure of MCTS remained unbroken. It has been shown that cells cultured as MCTS exhibit multidrug resistance (MDR) more relevant to solid tumors *in vivo* as compared to the cells grown in monolayer form *in vitro*.[1] Hence, the modification of micelles with penetration peptides (*e.g.*, RGD)[11] and targeting groups (*e.g.*, chemokine CXCR4 receptor)[44] might be a practical step in improving the antitumor efficacy of drug-loaded micelles.

Conclusions

Both crosslinked and uncrosslinked P(HPMA-*co*-MAA)-*b*-PMMA micelles were used to study the micelle penetration in MCTS. This research discovered the possible penetration pathway of PHPMA-based micelles from the peripheral layer into the inner section of pancreatic MCTS. It was found that the penetration is highly dependent on cellular activity. The micelles were initially taken up by the peripheral cells through endocytosis before being released inside the MCTS via exocytosis. This process is then repeated by the next "layer" of cells, accounting for the deeper penetration exhibited by the micellar systems, when compared to free drug. As a result of this transcellular penetration pathway, the stability of micelles plays a crucial role in the penetration in MCTS. Fast disassembly of uncrosslinked PHPMA-based micelles and quick release of the loaded drug can provoke the apoptosis of peripheral cells and cease the transport from outer part to inner part of MCTS.

Acknowledgements

Notes and references

a Centre for Advanced Macromolecular Design, School of Chemistry, University of New South Wales, Kensington, Sydney, New South Wales 2052, Australia, E-mail: M.Stenzel@unsw.edu.au
b School of Chemical Engineering, University of New South Wales, Kensington, Sydney, New South Wales 2052, Australia.

† Electronic Supplementary Information (ESI) available: [Cytotoxicity test methods and results for polymer and inhibitors, NMR spectrum of copolymers, and Microphotographs of pancreatic spheroids before and after DOX-loaded micelles treatment]. See DOI: 10.1039/b000000x/

1. N. R. Patel, B. S. Pattni, A. H. Abouzeid and V. P. Torchilin, *Adv. Drug. Deliv. Rev.*, 2013, **65**, 1748-1762.
2. V. P. Torchilin, *Adv. Drug. Deliv. Rev.*, 2012, **64**, S302-315.
3. V. P. Torchilin, *Nat. Rev. Drug Discov.*, 2014, **13**, 813-827.
4. R. Savic, L. B. Luo, A. Eisenberg and D. Maysinger, *Science*, 2003, **300**, 615-618.
5. R. K. Jain and T. Stylianopoulos, *Nat. Rev. Clin. Oncol.*, 2010, **7**, 653-664.
6. N. Nishiyama and K. Kataoka, *Pharmocol. Ther.*, 2006, **112**, 630-648.
7. Y. Matsumura, T. Hamaguchi, T. Ura, K. Muro, Y. Yamada, Y. Shimada, K. Shirao, T. Okusaka, H. Ueno, M. Ikeda and N. Watanabe, *Brit. J. Cancer.*, 2004, **91**, 1775-1781.
8. H. Cabral, Y. Matsumoto, K. Mizuno, Q. Chen, M. Murakami, M. Kimura, Y. Terada, M. R. Kano, K. Miyazono, M. Uesaka, N. Nishiyama and K. Kataoka, *Nat. Nanotechnol.*, 2011, **6**, 815-823.
9. W. Scarano, H. T. T. Duong, H. X. Lu, P. L. De Souza and M. H. Stenzel, *Biomacromolecules*, 2013, **14**, 962-975.
10. H. Xin, X. Sha, X. Jiang, W. Zhang, L. Chen and X. Fang, *Biomaterials*, 2012, **33**, 8167-8176.
11. G. Gu, X. Gao, Q. Hu, T. Kang, Z. Liu, M. Jiang, D. Miao, Q. Song, L. Yao, Y. Tu, Z. Pang, H. Chen, X. Jiang and J. Chen, *Biomaterials*, 2013, **34**, 5138-5148.
12. G. Mehta, A. Y. Hsiao, M. Ingram, G. D. Luker and S. Takayama, *J. Control. Release*, 2012, **164**, 192-204.
13. S. M. Ong, Z. Zhao, T. Arooz, D. Zhao, S. Zhang, T. Du, M. Wasser, D. van Noort and H. Yu, *Biomaterials*, 2010, **31**, 1180-1190.
14. R. Z. Lin and H. Y. Chang, *Biotechnol. J.*, 2008, **3**, 1172-1184.
15. F. Perche, N. R. Patel and V. P. Torchilin, *J. Control. Release*, 2012, **164**, 95-102.
16. Q. Hu, X. Gao, T. Kang, X. Feng, D. Jiang, Y. Tu, Q. Song, L. Yao, X. Jiang, H. Chen and J. Chen, *Biomaterials*, 2013, **34**, 9496-9508.
17. A. Bandekar, S. Karve, M.-Y. Chang, Q. Mu, J. Rotolo and S. Sofou, *Biomaterials*, 2012, **33**, 4345-4352.
18. Q. Zhang, J. Tang, L. Fu, R. Ran, Y. Liu, M. Yuan and Q. He, *Biomaterials*, 2013, **34**, 7980-7993.
19. Y. Gao, M. Li, B. Chen, Z. Shen, P. Guo, M. G. Wientjes and J. L. S. Au, *AAPS J.*, 2013, **15**, 816-831.
20. K. Huang, H. Ma, J. Liu, S. Huo, A. Kumar, T. Wei, X. Zhang, S. Jin, Y. Gan, P. C. Wang, S. He, X. Zhang and X. J. Liang, *ACS Nano*, 2012, **6**, 4483-4493.
21. S. M. Sagnella, H. Duong, A. MacMillan, C. Boyer, R. Whan, J. A. McCarroll, T. P. Davis and M. Kavallaris, *Biomacromolecules*, 2014, **15**, 262-275.
22. A. I. Minchinton and I. F. Tannock, *Nat. Rev. Cancer.*, 2006, **6**, 583-592.
23. Y. Kim, M. H. Pourgholami, D. L. Morris and M. H. Stenzel, *Biomacromolecules*, 2012, **13**, 814-825.
24. N. M. Barkey, C. Preihs, H. H. Cornnell, G. Martinez, A. Carie, J. Vagner, L. Xu, M. C. Lloyd, V. M. Lynch, V. J. Hruby, J. L. Sessler, K. N. Sill, R. J. Gillies and D. L. Morse, *J. Med. Chem.*, 2013, **56**, 6330-6338.
25. M. Talelli, C. J. F. Rijcken, C. F. van Nostrum, G. Storm and W. E. Hennink, *Adv. Drug Deliv. Rev.*, 2010, **62**, 231-239.
26. H. T. T. Duong, T. L. Uyen Nguyen and M. H. Stenzel, *Polym. Chem.*, 2010, **1**, 171-182.
27. Y. Kim, M. H. Pourgholami, D. L. Morris, H. Lu and M. H. Stenzel, *Biomater. Sci.*, 2013, **1**, 265-275.
28. C. Sanson, C. Schatz, J.-F. Le Meins, A. Soum, J. Thévenot, E. Garanger and S. Lecommandoux, *J. Control. Release*, 2010, **147**, 428-435.
29. Y. T. Matsunaga, Y. Morimoto and S. Takeuchi, *Adv. Mater.*, 2011, **23**, H90-H94.
30. Z. Zhang, Q. Qu, J. Li and S. Zhou, *Macromol. Biosci.*, 2013, **13**, 789-798.
31. S. E. A. Gratton, P. A. Ropp, P. D. Pohlhaus, J. C. Luft, V. J. Madden, M. E. Napier and J. M. DeSimone, *Proc. Natl. Acad. Sci. USA*, 2008, **105**, 11613-11618.

32. L. Yu, L. Yao, J. You, Y. Guo and L. Yang, *J. Appl. Polym. Sci*, 2014, **131**, 39623.

33. H. Hillaireau and P. Couvreur, *Cell. Mol. Life Sci.*, 2009, **66**, 2873-2896.

34. Y. Feng, S. Yu, T. K. R. Lasell, A. P. Jadhav, E. Macia, P. Chardin, P. Melancon, M. Roth, T. Mitchison and T. Kirchhausen, *Proc. Natl. Acad. Sci. USA*, 2003, **100**, 6469-6474.

35. M. F. Serag, N. Kaji, E. Venturelli, Y. Okamoto, K. Terasaka, M. Tokeshi, H. Mizukami, K. Braeckmans, A. Bianco and Y. Baba, *ACS Nano*, 2011, **5**, 9264-9270.

36. K. L. Sodek, M. J. Ringuette and T. J. Brown, *Int. J. Cancer*, 2009, **124**, 2060-2070.

37. S. Kim, Y. Shi, J. Y. Kim, K. Park and J.-X. Cheng, *Expert Opin. Drug. Deliv.*, 2010, **7**, 49-62.

38. W. Jiang, B. Y. S. Kim, J. T. Rutka and W. C. W. Chan, *Nat. Nanotechnol.*, 2008, **3**, 145-150.

39. A. Albanese, A. K. Lam, E. A. Sykes, J. V. Rocheleau and W. C. Chan, *Nat. Commun.*, 2013, **4**, 2718.

40. T. T. Goodman, P. L. Olive and S. H. Pun, *Int. J. Nanomed.*, 2007, **2**, 265-274.

41. M. Magzoub, S. Jin and A. S. Verkman, *FASEB J.*, 2008, **22**, 276-284.

42. Y. Li, H. He, X. Jia, W.-L. Lu, J. Lou and Y. Wei, *Biomaterials*, 2012, **33**, 3899-3908.

43. X. Wang, X. Zhen, J. Wang, J. Zhang, W. Wu and X. Jiang, *Biomaterials*, 2013, **34**, 4667-4679.

44. S. Singh, S. K. Srivastava, A. Bhardwaj, L. B. Owen and A. P. Singh, *Brst. J. Cancer*, 2010, **103**, 1671-1679.